Draft version February 23, 2015
Preprint typeset using LATEX style emulateapj v. 5/2/11

arXiv:1502.05823v1 [astro-ph.GA] 20 Feb 2015

A COMPLETE CENSUS OF SILICATE FEATURES IN THE MID-INFRARED SPECTRA OF ACTIVE GALAXIES

E. Hatziminaoglou[1], A. Hernán-Caballero[2], A. Feltre[3], and N. Piñol-Ferrer[4]
[1]ESO, Karl-Schwarzschild-Str. 2, 85748 Garching bei München, Germany, ehatzimi@eso.org
[2]Instituto de Física de Cantabria, CSIC-UC, Avenida de los Castros s/n, 39005, Santander, Spain
[3]Institut d'Astrophysique de Paris, 98 bis boulevard Arago, 75014 Paris, France and
[4]Department of Astronomy, Stockholm University, AlbaNova Center, 106 91 Stockholm, Sweden

Draft version February 23, 2015

ABSTRACT

We present a comprehensive study of the silicate features at 9.7 and 18 μm of a sample of almost 800 active galactic nuclei (AGN) with available spectra from the *Spitzer* InfraRed Spectrograph (IRS). We measure the strength of the silicate feature at 9.7 μm, $S_{9.7}$, before and after subtracting the host galaxy emission from the IRS spectra. The numbers of type 1 and 2 AGN with the feature in emission increase by 20 and 50%, respectively, once the host galaxy is removed, while 35% of objects with the feature originally in absorption exhibit it in even deeper absorption. The peak of $S_{9.7}$, $\lambda_{\rm peak}$, has a bimodal distribution when the feature is in emission, with about 65% of the cases showing $\lambda_{\rm peak} > 10.2$ μm. Silicates can appear in emission in objects with mid-infrared (MIR) luminosity spanning over six orders of magnitude. The derived distributions of the strength of the silicate features at 9.7 and 18 μm provide a solid test bed for modeling the dust distribution in AGN. Clumpiness is needed in order to produce absorption features in unobscured AGN and can also cause the silicates to be in absorption at 9.7 μm and in emission at 18 μm in type 1 sources. We find the 'cosmic' silicates of Ossenkopf et al. to be more consistent with the observations than Draine's 'astronomical' silicates. Finally, we discuss the possibility of a foreground absorber to explain the deep silicate absorption features in the MIR spectra of some type 2 AGN.

Subject headings: galaxies: active — infrared: galaxies

1. INTRODUCTION

The InfraRed Spectrograph (IRS; Houck et al. 2004) onboard the *Spitzer* Space telescope provided, over a period of more than five years, low- and high-resolution mid-infrared (MIR) spectra from many thousands of galactic and extragalactic sources, at wavelengths between 5 and 40 μm.

In active galactic nuclei (AGN), the MIR emission is believed to be UV light reprocessed by the hot dust surrounding the AGN. The dust, often assumed to form a toroidal structure in parsec scales around the nucleus in a plain extending that of the accretion disk, is considered to be distributed either smoothly (e.g. Pier & Krolik 1992; Granato & Danese 1994; Fritz et al. 2006) or in clumps (e.g. Hönig et al. 2006; Nenkova et al. 2008). Dust is believed to consist of graphite and silicate grains, each leaving their unmistakable signature in the Spectral Energy Distribution (SED) of AGN, namely the ∼1500K black-body like rise of the MIR continuum of type (unobscured) AGN (e.g. Hatziminaoglou et al. 2005), corresponding to the sublimation temperature of graphites, and an absorption feature centred at 9.7 μm, long known to appear in type 2 (obscured) AGN, attributed to silicate grains.

The uncertain observational evidence for silicate in emission in type 1 AGN (Clavel et al. 2000), however, posed a problem for the Unified Scheme according to which the various types of AGN can be explained by alignment effects between the central sources, the obscuring material (torus) and the observer (Antonucci 1993). The problem was finally solved when silicates were unambiguously observed in emission in the MIR spectra of many known AGN with IRS (Siebenmorgen et al. 2005; Sturm et al. 2005; Hao et al. 2005; Buchanan et al. 2006; Shi et al. 2006).

Since then, various studies of the behaviour of the silicates have appeared. The very first such works, based on a few tens of AGN (e.g. Spoon et al. 2007; Hao et al. 2007; Wu et al. 2009), demonstrated that the silicate feature shows a wide diversity. On average spectra it varies with AGN type, ranging from moderate emission in bright quasars to almost no emission or slight absorption in Seyfert 1 galaxies to stronger absorption in Seyfert 2 galaxies. Meanwhile, sparse reports on the detection of silicates in emission (Mason et al. 2009; Nikutta et al. 2009) showed the diversity of the dust properties, albeit some of them rather rare. Several of the above observations also revealed a second silicate feature at 18 μm, as predicted by the models. The relative strength of the silicate features at 9.7 and 18 μm has been put forward as a possible diagnostic of the torus morphology (e.g. Thompson et al. 2009; Feltre et al. 2012) and chemistry (Sirocky et al. 2008).

In this paper, we put together the largest sample of active galaxies with available IRS spectra ever composed (Sec. 2) with the aim to complement and extend previous studies on the MIR characteristics of AGN. To this aim, we apply a new spectral decomposition technique to separate the nuclear emission from that of the host (Sec. 3). We then proceed with a thorough investigation of the behaviour of the silicate feature at 9.7 μm and 18 μm in the various AGN types (Sec. 4). Section 5 discusses our most important results and places them into a more general context.

TABLE 1
Number of objects per AGN type.

Type	$N_{\rm obj}$	Type	$N_{\rm obj}$
Type 1 AGN	363	Sy1.2	24
Type 2 AGN	325	Sy1.5	32
		Sy1.8	18
SDSS quasars	141	Sy1.9	22

2. THE SAMPLE

The Cornell AtlaS of *Spitzer*/Infrared Spectrograph project (CASSIS[1]; Lebouteiller et al. 2011) has made available the reduced spectra of all the sources observed with the low resolution modules of IRS, a total of about 11000 unique observations. Our master sample is derived from the CASSIS version 6 catalogue, keeping each object that fulfills the following requirements: i) has an identification in the NASA/IPAC Extragalactic Database[2] (NED); ii) has a robust (optical or infrared) spectroscopic redshift; iii) the IRS spectrum fully covers the range between 6 and 13 micron restframe; iv) the median signal-to-noise ratio (SNR) per pixel of the IRS spectrum is >2.

To verify requirement i) we rely on the source cross-identification from CASSIS, which matches the source coordinates with the NED and SIMBAD databases (Lebouteiller et al. 2011). For sources with no spectroscopic redshift in NED, we measure the redshift from the IRS spectrum using the template matching method presented in Hernán-Caballero (2012). The typical redshift uncertainty with this method is $\Delta z/(1+z) \sim 0.002$, well below the spectral resolution of our resampled spectra ($\Delta\lambda/\lambda$=0.005–0.02). The resampling also increases the minimum SNR per resolution element from 2 to > 3 (see Sec. 3).

Taking these criteria into account and removing duplicate entries, we end up with a list of 2299 extragalactic objects. Out of these, 784 objects have a NED classification as AGN of types 1, 2 or intermediate, and this is the sample we will be working with henceforth. AGN of undefined type were left out of the sample. Among the type 1 AGN lie 141 quasars from the Sloan Digital Sky Survey (SDSS) Data Release 7 Quasar Catalogue (Shen et al. 2011), that for few specific purposes will be examined separately. The numbers of the object per subsample are shown in Table 1. The AGN sample is heterogeneous but, nevertheless, representative of the infrared (IR) AGN population.

3. SPECTRAL DECOMPOSITION

The observed MIR spectra of AGN are affected by the presence of their host galaxies in two important ways. One is the absorption or scattering of AGN emissions by material (gas and dust) in the AGN line of sight. This so-called foreground absorption modulates the AGN spectrum with a multiplicative factor $e^{-\tau(\lambda)}$, where $\tau(\lambda)$ represents the optical depth at wavelength λ. It is not possible to distinguish foreground absorption from intrinsic AGN absorption (that is, the one produced in the AGN torus) from MIR data alone, since similar extinction laws are considered to apply to dust grains in the torus and the host. The amount of foreground extinction varies from source to source, but at MIR wavelengths it is expected to be mild in most sources, with the exception of some dusty starbursts and edge-on spiral galaxies. The other important effect on the AGN spectra is the contamination from host galaxy emission that blends with the AGN spectrum. The importance of this background emission depends on the relative luminosities of the AGN and the host and –crucially– on the spatial resolution of the spectroscopic observations. Since the emission from the AGN is typically unresolved, an increase in the spatial resolution implies that a larger fraction of the host emission can be resolved away. In any case, the background emission represents an additive modification to the AGN spectrum.

The purpose of our spectral decomposition is to separate the AGN and host emissions in the integrated AGN+host spectra. If successful, this decomposition allows to study the AGN emission as if the host galaxy was resolved away. To this aim we employ the decomposition method presented in Hernán-Caballero et al. (2015). The method relies on the large number of high-quality spectra in CASSIS to reproduce the spectra of composite sources as a linear combination of three CASSIS spectra, each selected from subsamples of sources whose mid-IR emission is completely dominated by the AGN, the star-formation, or the stellar population. We select these ‘single-spectral-component’ templates as follows:

For the ‘stellar’ templates, we select 19 local elliptical and S0 galaxies. To ensure they have negligible star formation, we require the Polycyclic Aromatic Hydrocarbons (PAH) bands to be very weak or absent, with equivalent widths for the 6.2 μm (EW_{62}) and 11.3 μm (EW_{113}) PAH features <0.02 μm. We also check that the IRS spectra have a blue stellar-like MIR continuum and the sources are not classified as AGN in NED. The 54 star-forming templates (‘PAH’ templates) are IRS spectra of normal star-forming and starburst galaxies at redshifts up to z=0.14. We make sure these sources do not have significant stellar contributions to their MIR spectra by requiring both high EW of the PAH features ($EW_{62} >$ 1.0 μm and $EW_{113} >$ 1.0 μm) and a very weak continuum at 5 μm. We also verify that they are not classified as AGN in NED. Finally, the 147 ‘AGN’ templates are IRS spectra of sources classified in the optical as quasars, Seyfert galaxies, LINERs, and blazars. We also include a variety of optically obscured AGN and radiogalaxies. The templates include sources at redshifts from z=0.002 to z=1.4 and cover several orders of magnitude in bolometric luminosity. We ensure that the AGN templates do not contain any significant emission from the host galaxy by requiring the PAH features to be extremely weak or absent ($EW_{62} <$ 0.02 μm and $EW_{113} <$ 0.02 μm).

Because the AGN and PAH templates are real spectra, each of them already includes some amount of foreground extinction built in. Therefore, we rely on the large number of AGN and PAH templates to reproduce the diversity of observed spectra that arises from different levels of foreground extinction as well as source to source variation in the intrinsic AGN and host spectra. This approach has the advantage of not depending on assumptions about the –unobservable– intrinsic AGN spectrum or the extinction law. Obtaining a good fit with this decomposition method requires finding an

---

[1] http://cassis.sirtf.com

[2] http://ned.ipac.caltech.edu

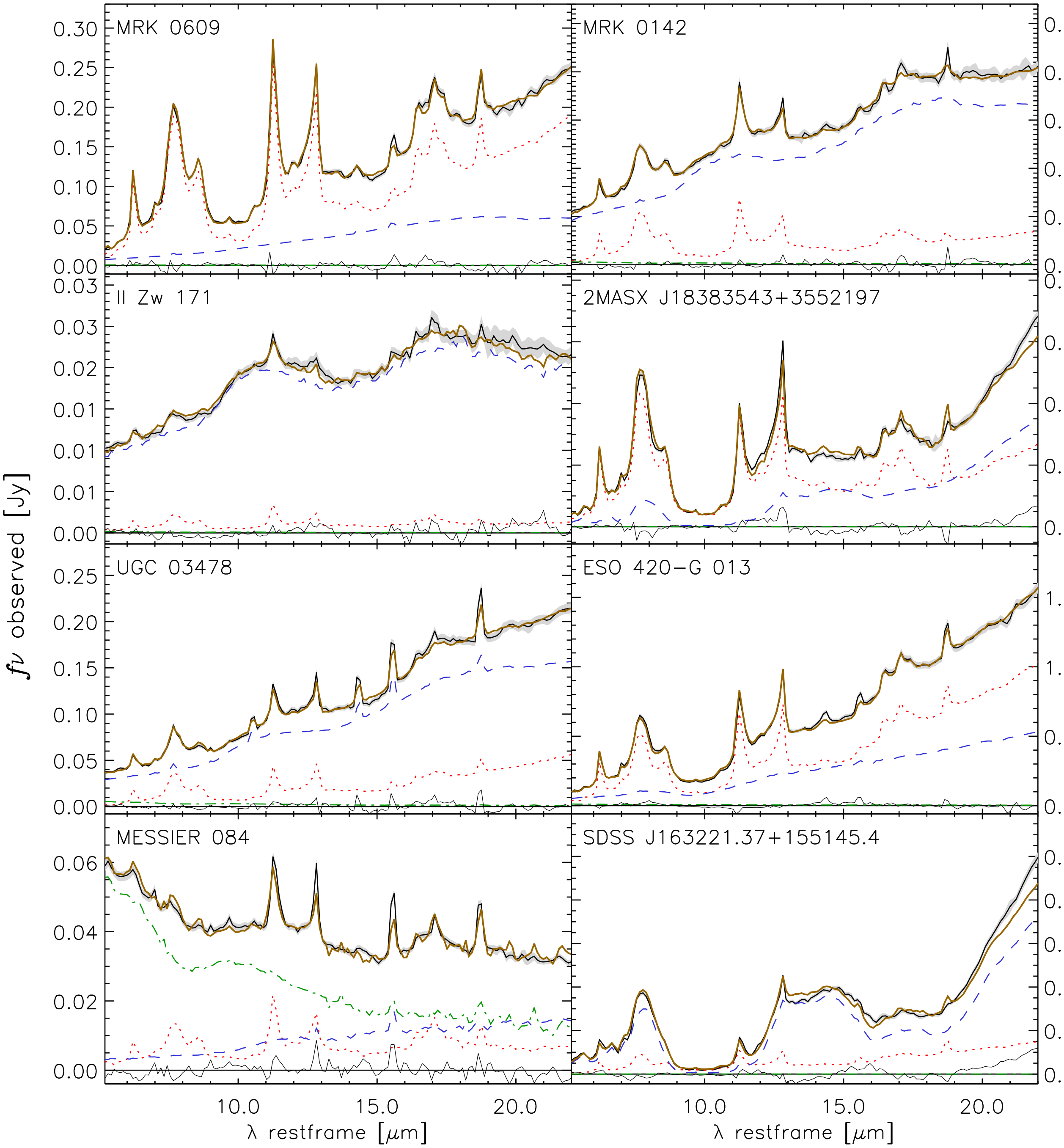

Fig. 1.— Examples of best-fitting decomposition models for the IRS spectra. The black solid line with grey shading represents the IRS spectrum (resampled at $\Delta\lambda$=0.1 μm resolution) and its 1-σ uncertainty (photometric errors only). The dotted, dashed, and dot-dashed lines represent, respectively, the PAH, AGN, and stellar components of the best-fitting model, shown in yellow. The thin solid line at the bottom of each plot represents the residual (spectrum - model).

AGN template with the appropriate level of foreground absorption. This can be problematic for sources with very deep absorption features, since few pure-AGN spectra have them. Accordingly, decomposition results for sources with deep absorption features have larger residuals and uncertainties.

We separate the AGN sample into two groups depending on the spectral coverage: those objects with silicate features observed both at 9.7 and at 18 μm in their full extent and those for which only the feature at 9.7 μm is covered. For sources in the first group, we fit the spectral range between 5.2 and 22 μm restframe, while for those in the second, we fit only the 5.2 to 15.8 μm range. We resample both the spectra and templates to a common wavelength grid with an uniform wavelength resolution of $\Delta\lambda$=0.1 μm. This increases the SNR per resolution element by ∼60% on average, while it still allows to resolve important features such as the PAH bands. For every galaxy in the sample we try spectral decompositions using every possible combination of a stellar template, a

PAH template, and an AGN template. The best fitting model is the one that produces the absolute minimum of χ^2. However, to calculate expected values for observables (e.g. the luminosity of the AGN component or the strength of the silicate feature) and their uncertainties, we use the full probability distribution functions (PDFs) calculated with the 'max' method described in Noll et al. (2009) (for details see Hernán-Caballero et al. 2015, Sec. 2). The method also yields, for each object, the fractional contribution of each the three components to the total luminosity, in the wavelength range of interest.

Thanks to the use of large sets of real spectra as templates, our decomposition method manages to reproduce the MIR spectrum of composite sources with unprecedented accuracy (see Fig. 1). Typical χ^2 values are lower than 2, indicating that residuals in the model fits are dominated by noise in both the spectra and templates for most sources.

4. THE SILICATE FEATURES

The silicate features at 9.7 and 18 µm observed in the IR spectra of AGN are believed to arise from the inner, hotter parts of the torus or the hot, illuminated side of the clumps. We define the strength of the silicate feature following Pier & Krolik (1992):

$$\mathrm{S}_\lambda = \ln \frac{\mathrm{F}(\lambda_{peak})}{\mathrm{F_c}(\lambda_{peak})} \tag{1}$$

where $\mathrm{F}(\lambda_{\mathrm{peak}})$ and $\mathrm{F_c}(\lambda_{\mathrm{peak}})$ are the flux densities of the spectrum and the underlying continuum at the peak wavelength of the features, λ_{peak}. A negative (positive) value indicates a feature in absorption (emission).

4.1. *The Silicate feature at 9.7 micron*

The top panel of Fig. 2 shows the distribution of the strength of the silicate feature at 9.7 µm as measured on the original IRS spectra, $\mathrm{S}_{9.7\ \mathrm{tot}}$, for type 1 and type 2 AGN (the 96 AGN of intermediate type are not included here and will be discussed separately).

As already observationally established in the past ten years, $\mathrm{S}_{9.7\ \mathrm{tot}}$ takes a wide range of values (e.g. Hao et al. 2007; Levenson et al. 2007; Spoon et al. 2007; Wu et al. 2009, just to name a few). The average spectra of type 1 AGN exhibit the feature in weak to moderate emission (see e.g. Hao et al. 2007; Wu et al. 2009), while those of type 2 AGN present the feature in absorption (Sturm et al. 2006; Schweitzer et al. 2008; Mason et al. 2009; Hernán-Caballero & Hatziminaoglou 2011). Individually, however, type 1 and type 2 AGN can show silicates in absorption and emission, respectively. In our sample of 698 type 1 and 2 AGN, 35% of the type 1 AGN present the feature in absorption and about 15% of the type 2 AGN show the feature in emission.

At the same time, when in emission, the peak of the feature is often shifted to wavelengths longer than 9.7 µm in the rest frame, while the shift affects much less the feature when in absorption, as already reported by e.g Shi et al. (2014). Fig. 3 shows the distribution of the shift, $\Delta\lambda_{\mathrm{peak}} = \lambda_{\mathrm{peak}} - 9.7$ µm, as a function of the fractional contribution of the AGN to the luminosity in the range between 5 and 15 µm, f_{AGN}, for type 1 and type 2 objects (filled and open symbols, respectively), colour-coded by $\mathrm{S}_{9.7\ \mathrm{tot}}$. Looking at the sample as a whole, 65% (20%) of the objects with the silicates in emission have their $\lambda_{\mathrm{peak}} > 10.2$ µm ($\lambda_{\mathrm{peak}} > 10.6$ µm), while the fraction of objects with the same amount of shift among the AGN with silicates in absorption is less than 3%. The shift to longer wavelenghts is largely associated to a silicate feature in emission, and this in turn only occurs in strongly AGN-dominated spectra.

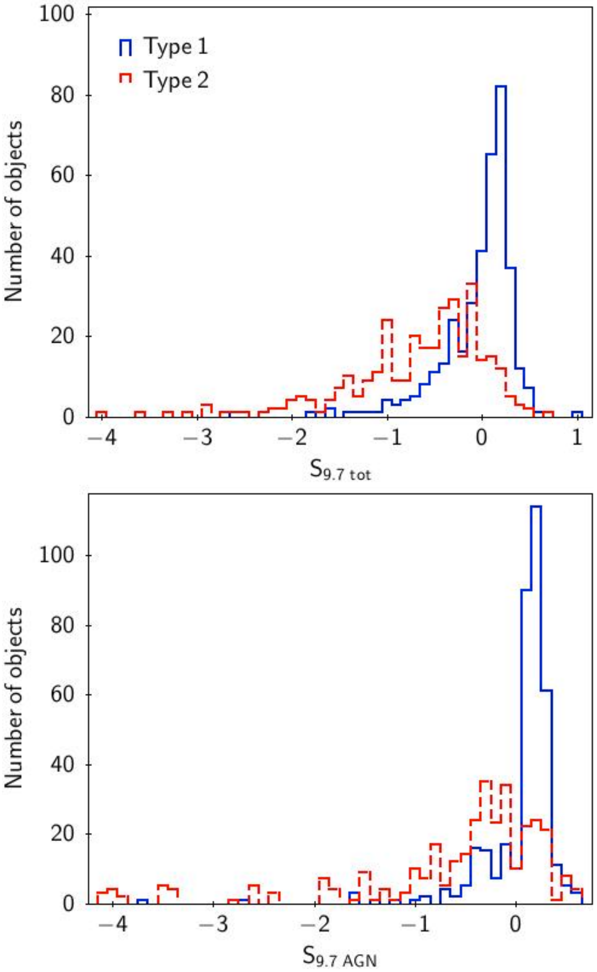

FIG. 2.— $\mathrm{S}_{9.7}$ distribution per for type 1 (blue solid histogram) and type 2 (red dashed histogram), before (top panel) and after (bottom panel) the subtraction of the host galaxy.

4.2. *Removing the effects of the host*

As $\mathrm{S}_{9.7\ \mathrm{tot}}$ are measured on the original IRS spectra, we expect the derived values to be contaminated by the emission of the host galaxy for all objects but those for which the AGN completely dominates the MIR emission. The top panel of Fig. 4 shows $\mathrm{S}_{9.7\ \mathrm{tot}}$ as a function of f_{AGN}. The filled and open symbols correspond to type 1 and type 2 AGN, respectively. Error bars for $\mathrm{S}_{9.7\ \mathrm{tot}}$ are shown in this plot but they will not be repeated in following figures, in order to keep the plots as little crowded as possible. What we see here is that as the contribution of the host becomes more important (i.e. as f_{AGN} decreases) the strength of the silicate feature decreases, with only few objects exhibiting $\mathrm{S}_{9.7\ \mathrm{tot}} > 0.0$ for $f_{\mathrm{AGN}} < 0.7$. The dashed line shows the (weak) trend for the full sample, with a linear correlation coefficient of r=0.45. The trend, however, is driven by type 1 objects

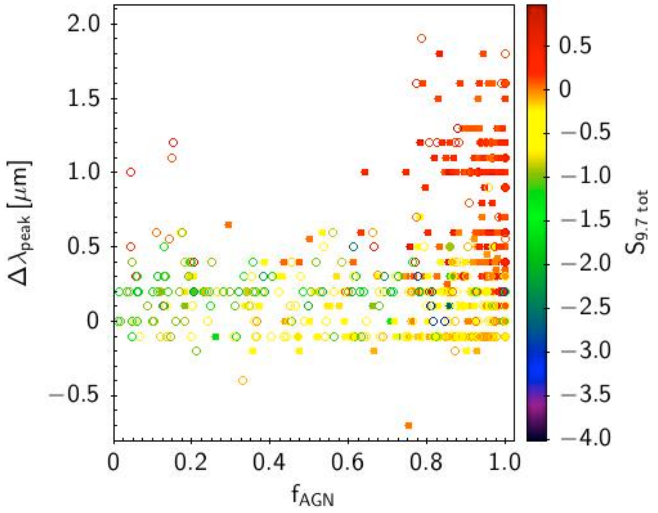

FIG. 3.— $\Delta\lambda_{\rm peak}$ as a function of $f_{\rm AGN}$, for type 1 and type 2 objects (filled and open symbols, respectively). The symbols are colour-coded based on the value of $S_{9.7\ \rm tot}$. The quantisation of $\Delta\lambda_{\rm peak}$ is an artifact of the algorithm that measures $\lambda_{\rm peak}$.

(filled symbols and corresponding solid line) due to the contamination by the emission of the host galaxy.

In order to see how the silicates behave in the vicinity of the nucleus, we need to remove the contribution of the host galaxy, applying the spectral decomposition procedure described in Sec. 3. The distribution of the strength of the silicate feature on the host-subtracted spectrum, $S_{9.7\ \rm AGN}$, is shown in the bottom panel of Fig. 2. The behaviour of $S_{9.7\ \rm AGN}$ with $f_{\rm AGN}$ shown in the lower panel of Fig. 4 differs from that of $S_{9.7\ \rm tot}$ in that there is now no correlation between the two quantities, confirming that the correlation was due to the contamination from the emission of the host, indeed.

A direct comparison of the two measurements of the silicate feature at 9.7 µm is shown in Fig. 5, colour-coded by the value of $f_{\rm AGN}$. Objects with MIR emission completely dominated by the AGN (light-colour symbols) are not affected by the subtraction of the host (they lie on or very near the 1:1 line). However, as the contribution of the host galaxy becomes more important, i.e. $f_{\rm AGN}$ decreases, (symbols become darker in Fig. 5), the points deviate more and more from the 1:1 line.

By subtracting the emission of the galaxy, the number of type 1 AGN with silicates in emission increases by 20%, reaching 80% of all type 1 AGN, while the number of type 2 AGN with the feature in emission doubles, reaching a total of 25%. At the same time, 35% of both type 1 and type 2 AGN with the feature in absorption exhibit the feature in even deeper absorption once the emission from the host is removed. This happens because AGN with a silicate feature in deeper absorption than that of the surrounding host get their silicate feature 'refilled' in the integrated spectrum.

In order to check whether $S_{9.7\ \rm AGN}$ is affected by the AGN luminosity, as proposed by e.g. Maiolino et al. (2007), we have to rely on the luminosity at 7 µm, L_7, that spans over six orders of magnitude in our sample. MIR luminosity in AGN has, in fact, been shown to tightly correlate with the X-ray luminosity (see e.g. Lutz et al. 2004; Horst et al. 2008; Mateos et al. 2015),

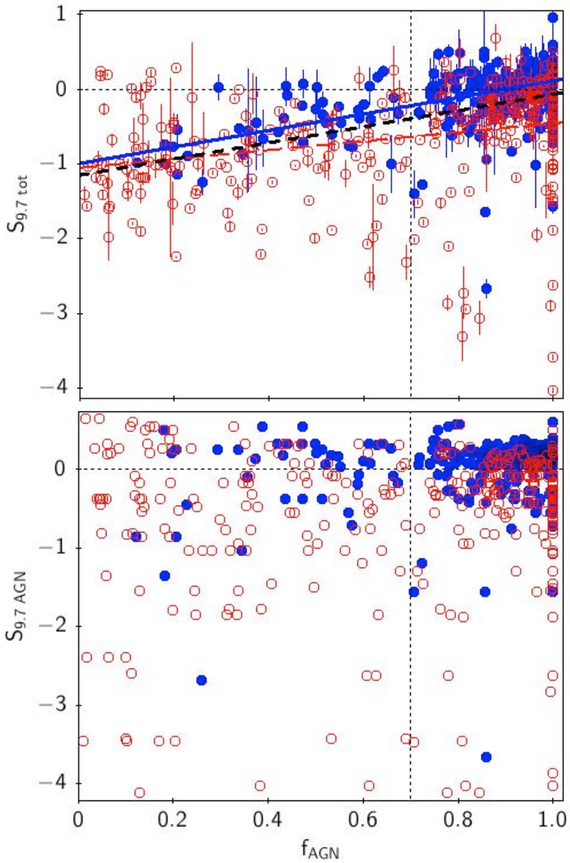

FIG. 4.— $S_{9.7}$ as a function of $f_{\rm AGN}$, before (upper panel) and after (lower panel) the subtraction of the host galaxy. Filled and open circles denote type 1 and type 2 AGN, respectively. The thin dashed lines show $S_{9.7}$=0.0 and $f_{\rm AGN}$=0.7, the thick dashed line shows the weak (r=0.45) linear correlation of the full sample, and the solid and long-dashed lines show the correlations for the type 1 (r=0.51) and type 2 (r=0.26) objects, respectively.

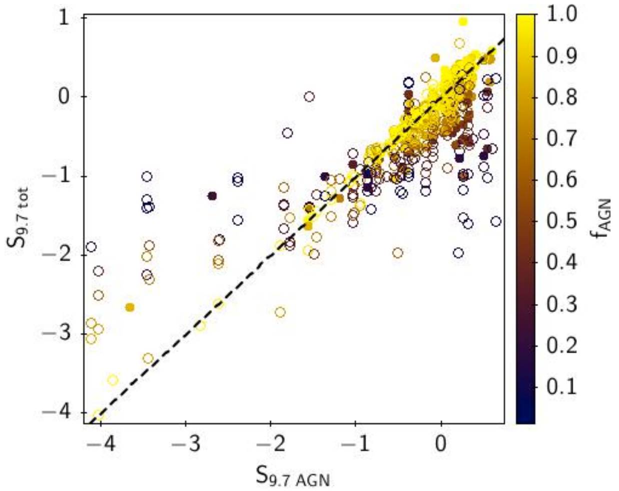

FIG. 5.— $S_{9.7\ \rm tot}$ versus $S_{9.7\ \rm AGN}$, colour-coded based on$f_{\rm AGN}$. Filled and open symbols denote type 1 and type 2 AGN, respectively.

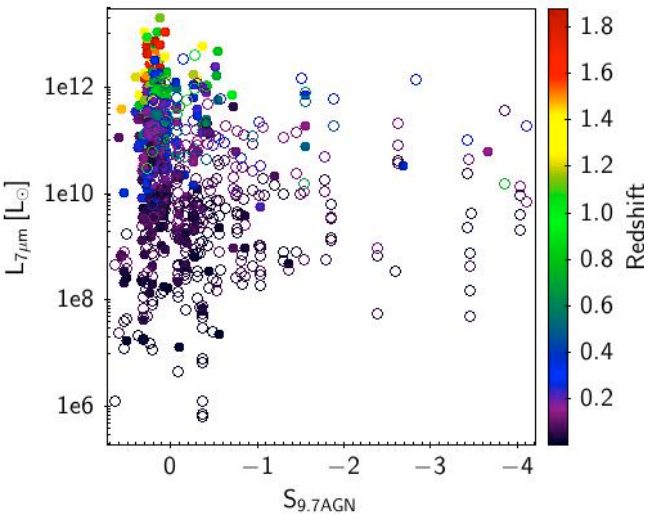

FIG. 6.— The relation between $S_{9.7\ \mathrm{AGN}}$ and L_7, with points colour-coded based on their redshift. The filled and open circles correspond to type 1 and type 2 AGN, respectively.

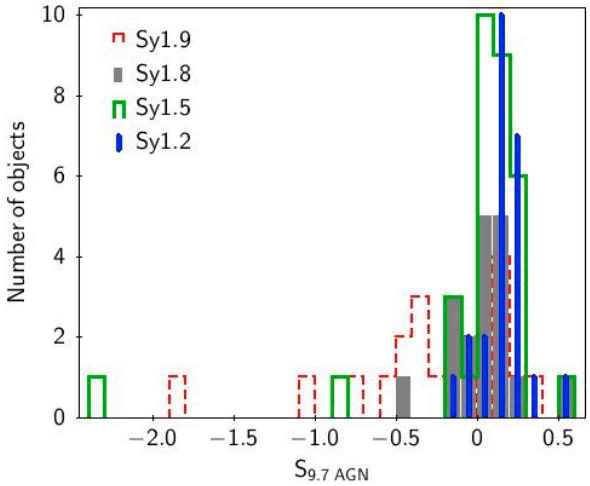

FIG. 7.— The distribution of $S_{9.7\ \mathrm{AGN}}$ for the four intermediate types of Seyfert galaxies.

TABLE 2
MEAN VALUES AND STANDARD DEVIATIONS OF $S_{9.7}$ FOR EACH INTERMEDIATE AGN TYPE, FRACTION OF OBJECTS WITH $f_{\mathrm{AGN}} > 0.7$ AND $S_{9.7}$ FOR THAT FRACTION.

Type	$\langle S_{9.7\ \mathrm{tot}} \rangle$	$f_{\mathrm{AGN}} > 0.7$	$\langle S_{9.7\ \mathrm{tot}}^{f_{\mathrm{AGN}}>0.7} \rangle$
Sy1.2	0.175±0.13	96%	0.160±0.14
Sy1.5	0.043±0.46	90%	0.087±0.22
Sy1.8	0.022±0.22	61%	0.059±0.11
Sy1.9	-0.305±0.49	55%	-0.227±0.35

the ratio of the MIR to the bolometric luminosity depends, however, on the column density along the line of sight (Fig. 21 in Hatziminaoglou et al. 2009). Fig. 6 shows $S_{9.7\ \mathrm{AGN}}$ as a function of L_7 measured on the galaxy-subtracted spectrum, with the points coloured based on the redshift. There is clearly no dependence of $S_{9.7\ \mathrm{AGN}}$ with L_7 and the features can be in emission ($S_{9.7} > 0.0$) even in the faintest AGN. Deep silicate features ($S_{9.7}$ <-2) are only found at intermediate luminosities (or redshifts). A deeply obscured but low-luminosity AGN would be overwhelmed by the emission of its host, that would 'refill' the silicate feature. The lack of deep silicates in objects with very high IR luminosities and/or high redshifts, on the other hand, suggests a selection effect, as they might be too faint in the optical for a reliable identification.

4.2.1. *AGN of intermediate types*

Among the 784 AGN of our sample, 96 have a NED classification of intermediate type Seyfert galaxies. The number of objects per type (comparable in all four subsamples) is shown in Table 1. Figure 7 shows the distribution of $S_{9.7\ \mathrm{AGN}}$ for the four sub-samples.

The mean average $S_{9.7\ \mathrm{AGN}}$ decreases from Sy1.2 towards later types, with Sy 1.2, 1.5 and 1.8 showing on average the silicate feature in very weak or no emission, while Sy1.9 has a negative average value. Additionally, as we move to later intermediate types, the dominance of the AGN component to the MIR emission decreases: while 96% of Sy1.2 objects have $f_{\mathrm{AGN}} > 0.7$, the fraction drops to 55% for Sy1.9s. This is in agreement with Deo et al. (2007) that found the MIR spectra of Sy1.8 and Sy1.9 to be dominated by starburst features (PAH). The mean values of $S_{9.7\ \mathrm{AGN}}$ and the fraction of objects with $f_{\mathrm{AGN}} > 0.7$ for each intermediate type are shown in Table 2. Note that the shift towards lower values of $S_{9.7\ \mathrm{AGN}}$ when moving towards later Seyfert types persist even when only objects with $f_{\mathrm{AGN}} > 0.7$ are considered, as seen in the right-most column of table 2. Finally, the λ_{peak} of intermediate Seyfert types shows the same behaviour as for the rest of the AGN sample, i.e. as described in Sec. 4.1.

4.2.2. *SDSS quasars*

Out of the 784 AGN, 141 are spectroscopically confirmed SDSS quasars, for which estimates of the mass of the central black hole, M_{BH}, derived from emission line measurements, as well as bolometric luminosities, L_{bol}, derived from fitting techniques are available (Shen et al. 2011). Maiolino et al. (2007) reported an increase of $S_{9.7}$ with increasing M_{BH}, from low-luminosity, low-redshift type 1 AGN to high-luminosity, high-redshift quasars. Thompson et al. (2009), on the other hand, found no trend of with luminosity. M_{BH} for the 141 SDSS quasars in question spans the range [$10^{7.3}$ $M_\odot$ – 10^{10} $M_\odot$], i.e. almost identical to that of the Maiolino et al. (2007) sample, but we do not find any correlation of $S_{9.7\ \mathrm{AGN}}$ with M_{BH}, as shown in Fig. 8. Note, however, that the bolometric luminosities of the SDSS quasars of our sample are all above 8.2 $\times 10^{10}$ $L_\odot$ ($10^{44.5}$erg/sec), i.e. the two samples are not directly comparable. In the quasar subsample, $S_{9.7\ \mathrm{AGN}}$ and L_{bol} are completely uncorrelated (see colour-coding in Fig. 8), in agreement with Thompson et al. (2009).

4.3. *The Silicate feature at 18 micron*

The silicate feature at 18 µm, though predicted by models and observed in many of the low-to-intermediate redshift AGN (z typically $\leq$ 0.5) by now (e.g. Hao et al. 2005; Sirocky et al. 2008; Thompson et al. 2009), has received less attention than its lower wavelength counterpart, as its measurement presents a greater challenge. For one, it often overlaps with the MIR bump of the

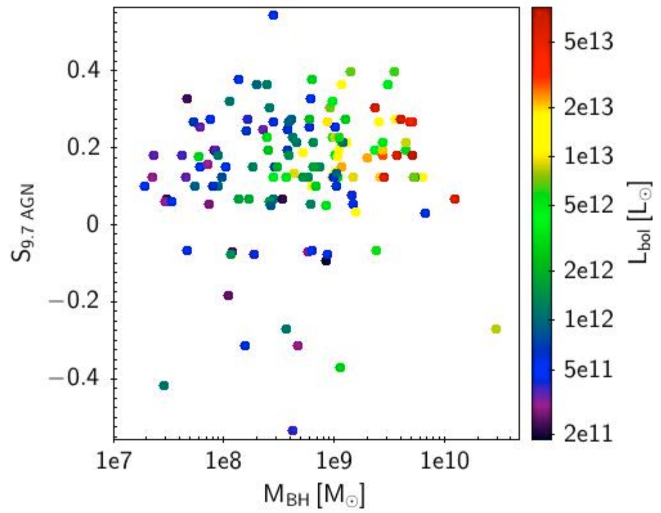

FIG. 8.— $S_{9.7\ \mathrm{AGN}}$ as a function of M_{BH} for the 141 SDSS quasars of the sample. The points are colour-coded by L_{bol}.

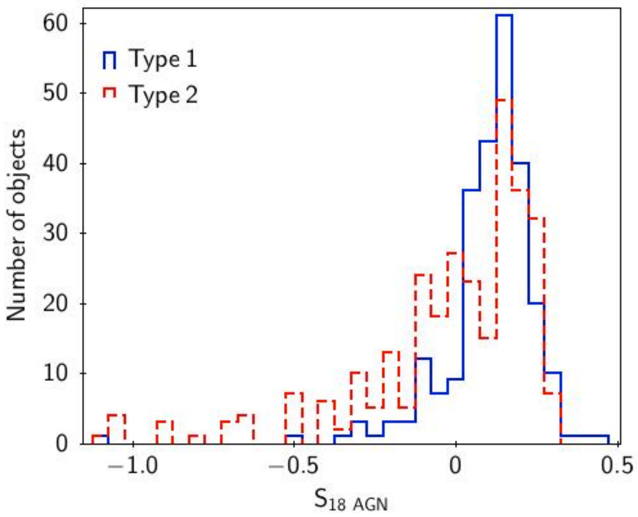

FIG. 9.— $S_{18\ \mathrm{AGN}}$ distribution per AGN type (type 1 in blue solid histogram, type 2 in red dashed histogram).

AGN SED (e.g. Prieto et al. 2010). Also, the steep mid-to-far IR emission from the host implies it contributes a higher fraction to the continuum emission at these longer wavelengths, making the measurement of the feature a tedious job. Following the procedure described in Sec. 3, but extending the wavelength range to 22 µm rest-frame, we perform spectral decompositions and measure the strength of the 18 µm silicate feature in the AGN component, $S_{18\ \mathrm{AGN}}$, for the 631 AGN with adequate wavelength coverage. Fig. 9 shows the distribution of $S_{18\ \mathrm{AGN}}$ for type 1 (blue solid histograms) and type 2 (red dashed histograms).

While at least as prominent as its counterpart at 9.7 µm in emission, when in absorption the feature only reaches moderate depths. Furthermore, more than 50% of type 2 AGN exhibit the feature in emission while only 10% of type 1 AGN have it in absorption. Comparing these numbers with those for $S_{9.7\ \mathrm{AGN}}$ it becomes obvious that the feature can be in absorption at 9.7 µm while still in emission at 18 µm. We will get back to this point in Sec. 5.

5. DISCUSSION AND CONCLUSIONS

Using the largest sample of AGN with MIR spectroscopy ever assembled we quantify, for the first time, the effects of the emission of the host galaxy on the behaviour of the silicate features, a tracer of the properties of the hot dust in the torus. We rely on the classification provided by NED in order to call an object "AGN" as well as for the classification of AGN in types 1 and 2. The sample includes a variety of AGN, from objects where the AGN completely dominates the MIR emission ($f_{\mathrm{AGN}} \sim 1$) to AGN whose MIR emission is almost entirely dominated by star formation ($f_{\mathrm{AGN}} << 1$). We find the fraction of objects with a strong contamination from the galaxy ($f_{\mathrm{AGN}} < 0.7$) to be much higher among type 2 AGN (43 pre cent) than among type 1 AGN (12 pre cent).

The emission of the host affects the behaviour of the silicate features. Broadly speaking, the strength of the silicate feature at 9.7 µm is a measure of the optical depth, $\tau_{9.7}$, along the line of sight, and goes from emission to absorption as $\tau_{9.7}$ increases (see e.g. Fritz et al. 2006, Fig. 9). In this simple picture, type 1 and type 2 AGN should show the feature in emission and absorption, respectively. Our study, however, shows that type 1 (type 2) AGN with the feature in absorption (emission) are very common, even after subtracting the contribution of the host galaxy. The numbers of type 1 and 2 AGN with the feature in emission increase by 20 and 50%, respectively, once the host galaxy is removed, while 35% of objects with the feature originally in absorption exhibit it in even deeper absorption after subtraction of the host. This means that the combined spectrum exhibits an $S_{9.7\ \mathrm{tot}}$ intermediate between $S_{9.7\ \mathrm{AGN}}$ and that of the host. The host galaxy nearly always shows mild silicate absorption, as the power sources (stars) are well mixed with the absorbing dust, and therefore the strength of the silicate feature does not correlate with the optical depth of the gas and dust along the line of sight. Consequently, contamination from the host increases the depth of the absorption if the feature intrinsic to the AGN is in emission or mild absorption, but decreases the depth (i.e. fills the gap) if the AGN has a deeper feature than the host.

$S_{9.7\ \mathrm{tot}}$ is scarcely ever shown in emission when the MIR emission is strongly contaminated by the host galaxy ($f_{\mathrm{AGN}} < 0.7$), with those objects exhibiting on average the feature in deeper absorption than their AGN-dominated counterparts. $S_{9.7\ \mathrm{AGN}}$, on the other hand, shows no dependency on f_{AGN} and appears from moderate emission to quite deep absorption with all possibilities in between. The lack of correlation between $S_{9.7\ \mathrm{AGN}}$ and f_{AGN}, two quantities that are physically unrelated, indicates that the decomposition mechanism successfully removes the most important part of the host galaxy emission, allowing for an almost unbiased silicate measurement of the silicate feature in the vicinity of the nucleus.

We have also addressed the issue of the observed shift of the silicate feature at 9.7 µm to longer wavelengths with respect to the nominal peak at 9.7 µm. Our decomposition method does not allow reliable estimate of λ_{peak} on the galaxy-subtracted spectra. We therefore rely on the measurement carried out on the original IRS spectra. We find the largest shifts ($\lambda_{\rm peak} > 10.2$ µm) to appear only in objects with an important AGN component ($f_{\rm AGN} > 0.7$) with the feature in emission, regardless of their type. When the feature is in absorption, and again irrespective of the type, it appears at or near its nominal wavelength ($\lambda_{\rm peak} < 10.2$ µm). Since its discovery, various scenarii have been proposed in order to explain this shift, such as the presence of porous dust (Li, Shi & Li 2008; Smith et al. 2010), the presence of different dust species (Markwick-Kemper et al. 2007), or radiative transfer effects (Nikutta et al. 2009). Shi et al. (2014), however, posit that this is not a radiative transfer effect but rather the effect of direct exposure of the silicates to the nuclear radiation, that modifies the size or the chemical composition of the grains, more along the lines of Smith et al. (2010).

5.1. *Dust distribution inside and outside the torus*

$S_{9.7\ \rm AGN}$ is seen in only moderate emission or slight absorption in most type 1 AGN, a behaviour that traditionally favours a clumpy morphology, both because smooth models often predict silicates in stronger emission than observed and because, with the exception of a couple of smooth model parameter combinations, only clumpiness can explain the feature in absorption in unobscured AGN. However, and even though not producing the feature in absorption, a continuous dust distribution can also give rise to silicates in only weak emission for a large variety of parameters, as shown in Fig. 4 of Feltre et al. (2012). Furthermore, Sirocky et al. (2008) showed that the use of the Ossenkopf et al. (1992) dust absorption and scattering coefficients result in considerably less prominent silicate emission features compared to other dust models like Draine (2003). We therefore interpret the behaviour of $S_{9.7\ \rm AGN}$ alone as favouring the Ossenkopf et al. (1992) over the Draine (2003) silicates, but this property alone cannot provide much insight into the morphology of the dust.

The transition of the mean values of $S_{9.7}$ from weak emission to absorption from Sy1.2 to Sy1.9 can be explained by either dust morphologies: in a smooth medium it can be attributed to an increase of the inclination (as measured from the poles) and hence the intervening material, with the silicate feature at 9.7 µm that arises from the inner, hotter parts of the torus, being increasingly blocked by the bulk of the dust as the viewing angle increases. In a clumpy medium, on the other hand, this could simply be attributed to different levels of obscuration along the line of sight, independently on the orientation.

The combined strength of the silicate features at 9.7 and 18 µm is sensitive to the chemistry and morphology of the dust surrounding the AGN, i.e. the torus (Sirocky et al. 2008; Thompson et al. 2009; Feltre et al. 2012). To test this, we created three grids of models, two clumpy and a smooth, following Nenkova et al. (2008) and Feltre et al. (2012), respectively. All three sets of models share the same the primary source, described in Nenkova et al. (2008). One of the clumpy grids was created using the silicates absorption and scattering coefficients from Draine (2003) while the other clumpy as well as the smooth grids were created using the Ossenkopf et al. (1992) silicates. The models have been created to have *matched* parameters, as defined in Feltre et al. (2012), i.e. each of the smooth models in the grid has an equivalent model (in terms of geometrical properties) in the clumpy grid. The parameter space explored by the model grids is briefly described in Appendix A.

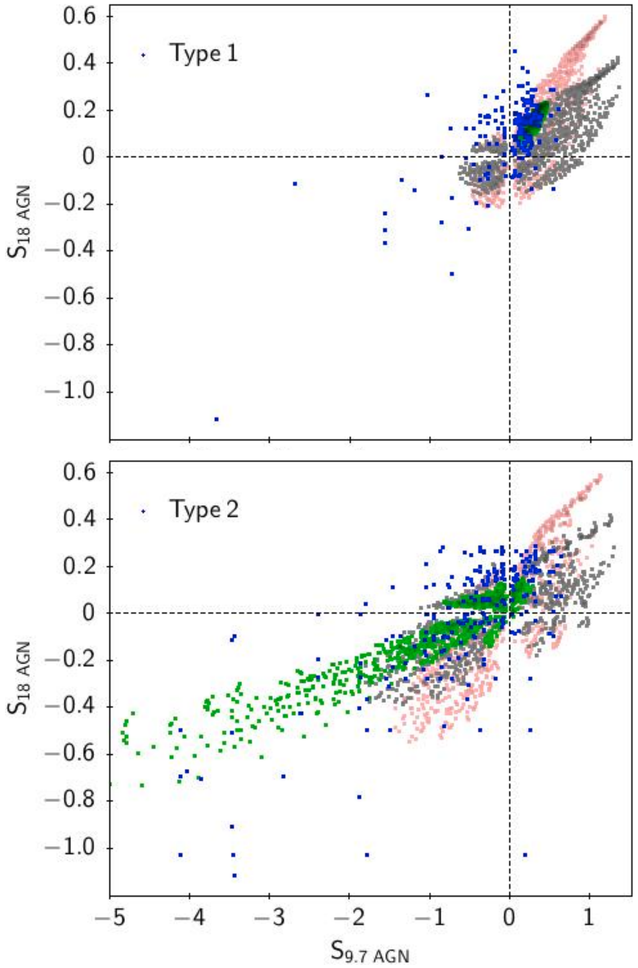

FIG. 10.— $S_{18\ \rm AGN}$ as a function of $S_{9.7\ \rm AGN}$, overplotted on model predictions. The top (bottom) panel shows type 1 (type 2) objects (in blue). Smooth models are shown in green, clumpy models with Ossenkopf et al. (1992) and Draine (2003) silicates are shown in grey and pink, respectively.

Fig. 10 shows the distributions of $S_{18\ \rm AGN}$ and $S_{9.7\ \rm AGN}$, compared to model predictions. The top (bottom) panel shows type 1 (type 2) AGN (in blue). Smooth models are shown in green, clumpy models using the Ossenkopf et al. (1992) and Draine (2003) silicates are shown in grey and pink, respectively. The spread of the observed data points indicates the variety of torus geometries in nature in terms of size, shape and optical depths.

As previously noted by other authors, the so called 'astronomical' silicates (Draine 2003) produce stronger emission features at 9.7 µm and a wider range of $S_{18\ \rm AGN}/S_{9.7\ \rm AGN}$ than what is observed, compared to the Ossenkopf et al. (1992) silicates. The bulk of type 1 objects lie in the region of overlap between smooth and clumpy models. Overall, models reproduce in a better fashion the silicates in type 2 AGN. However, both smooth and clumpy models, albeit covering a large parameter space, fail to reproduce the deep absorption features seen in type 1 AGN (lower left quadrant in top panel of Fig. 10). At the same time, and as already suggested by Imanishi et al. (2007), a continuous dust distribution is the only morphology that can reproduce the deepest absorption features seen in the sample for type 2 views (lower left quadrant of bottom panel in Fig. 10), at least without resorting to additional obscuration by the host galaxy. In fact, Levenson et al. (2007) suggested that a deep silicate absorption feature at 9.7 μm requires the primary source to be embedded in a continuous, optically and geometrically thick dusty medium, while a clumpy medium, with clouds illuminated from the outside, will result in a much shallower feature, as the emission from these clouds will fill the absorption trough.

We visually inspected all AGN with $S_{9.7\ \mathrm{AGN}} < -1.5$ for which we could find high enough resolution images and established that they are predominantly hosted in galaxies with high inclinations, galaxies with very visible dust lanes crossing the centre (e.g. NGC5793 or NGC7172), or reside in interactive systems at various stages of their interaction (e.g. Mkr 273, Mrk 331, NGC2623). In fact, Goulding et al. (2012) reach this same conclusion in their study of 20 nearby ($z < 0.05$) bona-fide Compton-thick AGN. This implies that the source of the deepest silicate absorption features is dust in the host galaxy rather than dust in the torus (see also Deo et al. 2007). In favour of this view, Lagos et al. (2011) find that type 1 AGN have a strong preference in residing in face-on galaxies, while the type 2 AGN reside in hosts of any orientation. The deep absorption features are, therefore, of no relevance to the modeling of the torus and they should not be used to favour smooth dust distributions over clumpy ones. We note that this is by no means an argument against the AGN unification scheme, but does suggest that the obscuration of the nucleus, i.e. a type 2 view, may, in some cases, be decoupled from the orientation of the torus.

Finally, what is not reproduce by none of the torus models are many of the obscured and unobscured AGN with the silicates absorption at 9.7 μm but in emission at 18 μm. Smooth models do not predict at all such a behaviour in type 1 views, while both morphologies produce $S_{18\ \mathrm{AGN}}$ of about half the strength than that measured on the spectra when $S_{9.7\ \mathrm{AGN}}$ is in absorption. Feltre et al. (2012) showed that the adopted primary source can also affect the properties of the silicate feature. As a last resort, and since we have no control of the primary source of the Nenkova models, we produced an additional grid of smooth models with the Ossenkopf et al. (1992) silicates but using the primary source from Feltre et al. (2012), that allows for more intrinsic AGN emission at wavelengths beyond 1 μm compared to the primary source used by the Nenkova et al. (2008) models, which we have adopted for the other grids. These models still fail to reproduce the objects in the upper left quadrant of the figure for type 1 views, they do however reproduce a much larger fraction of the objects in that same quadrant for type 2 views than any of the other model grids presented before, as shown in Fig. 11.

To summarise, and even though the emerging picture is still somewhat confusing, things start clearing up: the 'cosmic' silicates (Ossenkopf et al. 1992) represent in a satisfactory fashion the absorption and scattering properties of the silicates in the obscuring torus. Clumpiness is needed in order to produce absorption features in unobscured AGN, if no foreground absorber is invoked. Clumpiness can also cause the silicates to be in absorption at 9.7 μm and in emission at 18 μm in type 1 sources, but a primary source with more intrinsic AGN emission at $\lambda > 1.0$ μm might be necessary to create stronger $S_{18\ \mathrm{AGN}}$ in emission, when $S_{9.7\ \mathrm{AGN}} < 0.0$.

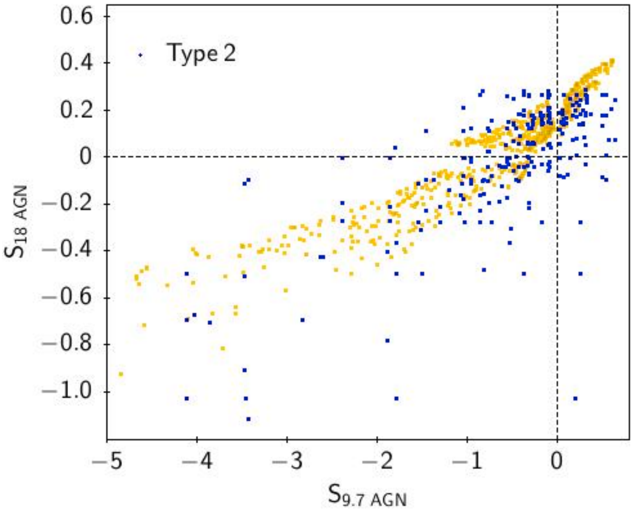

FIG. 11.— $S_{18\ \mathrm{AGN}}$ as a function of $S_{9.7\ \mathrm{AGN}}$ for type 2 objects (in blue), overplotted on smooth model predictions (in yellow), using the Feltre et al. (2012) primary source.

ACKNOWLEDGMENTS

The Cornell Atlas of *Spitzer*/IRS Sources (CASSIS) is a product of the Infrared Science Center at Cornell University, supported by NASA and JPL. We made use of the NASA/IPAC Extragalactic Database (http://ned.ipac.caltech.edu). We used the TOPCAT software written by Mark B. Taylor (http://www.star.bris.ac.uk/∼mbt/topcat/). AHC acknowledges support by the Universidad de Cantabria Augusto González Linares programme and the Spanish Plan Nacional de Astronomía y Astrofísica under grant AYA2012-31447. The research leading to these results has received funding from the European Research Council under the European Community's Seventh Framework Programme (FP7/2007-2013 Grant Agreement no. 321323).

APPENDIX

SMOOTH AND CLUMPY MODEL PARAMETERS

The two original smooth and clumpy model grids cover large but not entirely overlapping parameter space. For the purposes of this work, we *matched* the two sets of parameters to produce models that can be directly comparable. Both models share the inner-to-outer radius ratio, Y. The radial distribution of the dust or the clumps, q, can also

TABLE 3
Matched SMOOTH AND CLUMPY MODEL PARAMETERS.

	Smooth	Clumpy
Y	10, 30, 60, 100, 150	10, 30, 60, 100, 150
q	0, 1	0, 1
γ	1.65, 2.25, 3.24, 5.06, 9.0	
σ		$70°, 60°, 50°, 40°, 30°$
$\tau_{9.7}$	0.21, 0.42, 0.63, 0.84, 1.05, 1.26, 1.47, 1.68, 1.89, 2.1, 2.52, 2.94, 3.36, 3.78, 4.2, 5.04, 5.88, 6.3, 6.72, 7.56, 8.4, 10.08, 11.34, 11.76, 12.6	
N_0		1-5
τ_V		5, 10, 20, 30, 40, 60, 80, 100, 150

be considered as equivalent between the two models. For smooth models, the dust distribution in polar coordinates is given by:

$$\rho\left(r,\theta\right) = \rho_0 \cdot r^{-q} \cdot e^{-\gamma\times|\cos(\theta)|} \tag{A1}$$

while clumpy models assume a Gaussian angular distribution of clouds of width σ given by:

$$N_T(\beta) = N_0 \mathrm{e}^{(-\beta^2/\sigma^2)}, \tag{A2}$$

where N_0 is the average number of clouds along a given radial direction on the equatorial plain and β (=90-θ) is the angle with respect to the axis of the torus. Considering the two extreme viewing angles for both models, the torus opening angle is of no relevance and γ and σ can be taken such to match each other. While smooth models use the equatorial optical depth at 9.7 µm, $\tau_{9.7}$, as an input parameter, clumpy models use the optical depth of a single could calculated in the V-band at 0.55 µm, τ_V. $\tau_{9.7}$ for clumpy models can be derived via the relation $\tau_{9.7} = 0.042 \times \tau_V \times N_0$, (see Nenkova et al. 2008). Table 3 summarises the values of each of the parameters for the *matched* model grids.

REFERENCES

Antonucci R. 1993, ARA&A, 31, 473
Buchanan C. L., Gallimore J. F., O'Dea C. P. et al. 2006, AJ, 132, 401
Clavel J., Schulz B., Altieri B.et al. 2000, A&A, 357, 839
Deo R. P., Crenshaw D. M., Kraemer S. B. et al. 2007, ApJ, 671, 124
Draine B. T. 2003, ApJ, 598, 1017
Feltre A., Hatziminaoglou E., Fritz J., Franceschini A. 2012, MNRAS, 426, 120
Fritz J., Franceschini A., Hatziminaoglou E. 2006, MNRAS, 366, 767
Goulding A. D., Alexander D. M., Bauer F. E. et al. 2012, ApJ, 755, 5
Granato G.L., Danese L. 1994, MNRAS, 268, 235
Hao L., Weedman D. W. Spoon H. W. W. et al. 2007, ApJL, 655, L77
Hao L., Spoon H. W. W., Sloan G.C. et al. 2005, ApJL, 625, L75
Hatziminaoglou E., Fritz J., Jarrett T. 2009, MNRAS, 399, 1206
Hatziminaoglou E., Pérez-Fournon I., Polletta M. et al. 2005, AJ, 129, 1198
Hernán-Caballero A., Alonso-Herrero A., Hatziminaoglou E. et al 2015, ApJ, in press
Hernán-Caballero A. 2012, MNRAS, 427, 816
Hernán-Caballero A. & Hatziminaoglou E. 2011, MNRAS, 414, 500
Hernán-Caballero A., Pérez-Fournon I., Hatziminaoglou E. et al. 2009, MNRAS, 395, 1695
Hiner K. D., Canalizo G., Lacy M. et al. 2009, ApJ, 706, 508
Hönig S.F., Beckert T., Ohnaka K. et al. 2006, A&A, 452, 459
Horst H., Gandhi P., Smette A., Duschl W. J. 2008, A&A, 479, 389
Houck, J. R., Roellig, T. L., van Cleve, J., et al. 2004, ApJS, 154, 18
Imanishi M., Dudley C. C., Maiolino R. et al. 2007, ApJS, 171, 72
Lagos C., Padilla N. D., Strauss M. A., Cora S. A., Hao L. 2011, MNRAS, 414, 2148
Lebouteiller V., Barry D.J., Spoon H.W.W. et al. 2011, ApJS, 196, 8
Levenson N. A., Sirocky M. M., Hao L. et al. 2007, ApJL, 654, L45
Li M. P., Shi Q. J., Li A. 2008, MNRAS, 391, L49
Lutz D., Maiolino R., Spoon H. W. W., Moorwood A. F. M. 2004, A&A, 418, 465
Maiolino R., Shemmer O., Imanishi M. et al. 2007, A&A, 468, 979
Markwick-Kemper F., Gallager S. C., Hines D. C., Bouwman J. 2007, ApJL, 668, L107
Mason R. E., Levenson N. A., Shi Y. et al. 2009, ApJL, 693, L136
Mateos S., Carrera F. J., Alonso-Herrero A.et al. 2015, MNRAS, in press
Nenkova M., Sirocky M. M., Ivezić Ž., & Elitzur M. 2008, ApJ, 685, 147
Nikutta R., Elitzur M., & Lacy M. 2009, ApJ, 707, 1550
Noll S., Burgarella D., Giovannoli E. et al. 2009, A&A, 507, 1793
Ossenkopf V., Henning T., & Mathis J. S. 1992, A&A, 261, 567
Pier E.A. & Krolik J.H. 1992, ApJ, 401, 99
Prieto M. A., Reunanen J., Tristram K. R. W. et al. 2010, MNRAS, 402, 724
Schweitzer M., Groves B., Netzer H. et al. 2008, ApJ, 679, 101
Shen Y., Richards G. T., Strauss M. A. et al. 2011, ApJS, 194, 45
Shi Y., Rieke G. H., Ogle P. M., Su K. Y. L., Balog Z. 2014, ApJS, 214, 23
Shi Y., Rieke G. H., Hines D. C. et al. 2006, ApJ, 653, 127
Siebenmorgen R., Haas M., Krügel E., Schulz B. 2005, A&A, 436, L5
Sirocky M. M., Levenson N. A., Elitzur M., Spoon H. W. W., & Armus L. 2008, ApJ, 678, 729
Smith H. A., Li A., Li M. P. et al. 2010, ApJ, 716, 490
Smith J. D. T., Draine B. T., Dale D. A. et al. 2007, ApJ, 656, 770
Spoon H.W.W., Marshall J.A., Houck J.R. et al. 2007, ApJ, 654, L49
Sturm E., Hasinger G., Lehmann I. et al. 2006, ApJ, 642, 81
Sturm E., Schweitzer M., Lutz D. et al. 2005, ApJL, 629, L21
Thompson G. D., Levenson N. A., Uddin S. A., & Sirocky M. M. 2009, ApJ, 697, 182
Wu Y., Helou G., Armus L. et al. 2010, ApJ, 723, 895

Wu Y., Charmandaris V., Huang, J., Spinoglio, L., Tommasin, S. 2009, ApJ, 701, 658